American Mineralogist, Volume 71, pages 1322–1336, 1986

Complex exsolution in inverted pigeonite: Exsolution mechanisms and temperatures of crystallization and exsolution

WILLIAM A. RANSON
Department of Geology, Furman University, Greenville, South Carolina 29613, U.S.A.

ABSTRACT

The results of electron-microprobe and optical examination of Ca-poor pyroxenes from anorthositic and intermediate rocks of the Nain complex, Labrador, show a range in host composition from 100Fe/(Fe + Mg) = 34 to 77 and three distinct exsolution types. Type 1 pyroxenes have Bushveld-type exsolution with fine (100) augite lamelle and were primary orthopyroxenes. Type 2 and type 3 pyroxenes are inverted pigeonite with Stillwater-type exsolution. Type 2 varieties display irregular and unoriented lamellae and blebs of augite. Type 3 pyroxenes show complex exsolution features including broad "001" and "100" augite lamellae, multiple sets of pigeonite lamellae exsolving from "001" augite, fine (100) augite lamellae, and patches of uninverted pigeonite. Stacking faults, which are present in orthopyroxene and pigeonite host and "001" augite lamellae, bend 2–4° in a counterclockwise direction as they pass from host into "001" augite.

Exsolution occurred by the mechanism of nucleation and growth for all three pyroxene types. Observations suggest that homogeneous nucleation produced exsolution in type 1 and type 3 pyroxenes but that heterogeneous nucleation is responsible for the irregular exsolution in type 2 pyroxenes. Conventional estimates of crystallization temperatures are unrealistically low for type 1 pyroxenes, probably because of granule exsolution that produced discrete pyroxenes that were not included in microprobe analyses. Type 2 and type 3 pyroxenes crystallized at temperatures between 1100 and 1000°C at approximately 3-kbar pressure and began to exsolve augite. During initial cooling, strain developed along augite-pigeonite interphase boundaries, and stacking faults formed to relieve the strain. Fine stacking faults that propagated into the host from augite lamellae provided the mechanism for the pigeonite to orthopyroxene transformation. Some constrained patches of host pigeonite failed to invert. Coarse augite exsolution continued down to temperatures perhaps as low as 600°C. Pigeonite exsolution in "001" augite likely began before inversion and continued metastably to low but uncertain temperatures.

INTRODUCTION

Pyroxenes that have exsolved during cooling have been reported in both igneous and metamorphic rocks from a wide variety of environments of formation. Recently, considerable attention has been given to the orientation of exsolution lamellae with respect to the host crystal. Jaffe and Jaffe (1973) studied pyroxene granulites of the Monroe quadrangle in the Hudson Highlands of New York and reported three sets of lamellae in augites. Of these lamellae, only one set had a crystallographic axis that coincided with a crystallographic axis of the host, in this case the c axis. Optical observations of grain mounts confirmed that the remaining two sets of lamellae were not parallel to the (100) and (001) directions as proposed by Poldervaart and Hess (1951). Since this study, more detailed investigations of exsolution features have been made by Robinson et al. (1971), Jaffe et al. (1975), and by Robinson et al. (1977), who made use of single-crystal X-ray photographs to confirm the structures of lamellae and to develop the principle of the optimal phase boundary (Bollman and Nissen, 1968) to explain the irrational orientations commonly taken by exsolution lamellae. The first of these studies confirmed that (100) lamellae in augite hosts were orthopyroxene and that the other two sets were in fact pigeonite, which were designated as "001" and "100" lamellae, after the usage of Robinson et al. (1971), which refers to orientations not quite parallel to (100) and (001), respectively. Jaffe et al. (1975) described exsolution lamellae in various metamorphic augites and related the orientation of the lamellae to composition. Robinson et al. (1977) turned their attention from metamorphic to igneous augites, which experienced slow cooling from high temperature. They showed that the orientation of exsolution lamellae in igneous augites is dependent on high-temperature lattice parameters and suggested that lamellae orientation can be an effective geothermometer.

The present study describes a wide variety of exsolution types in Ca-rich and Ca-poor pyroxenes, with emphasis on augite exsolution in inverted pigeonite, and presents optical and microprobe data on pyroxenes as well. All of the pyroxenes discussed in this report are from the Nain

0003–004X/86/1112–1322$02.00

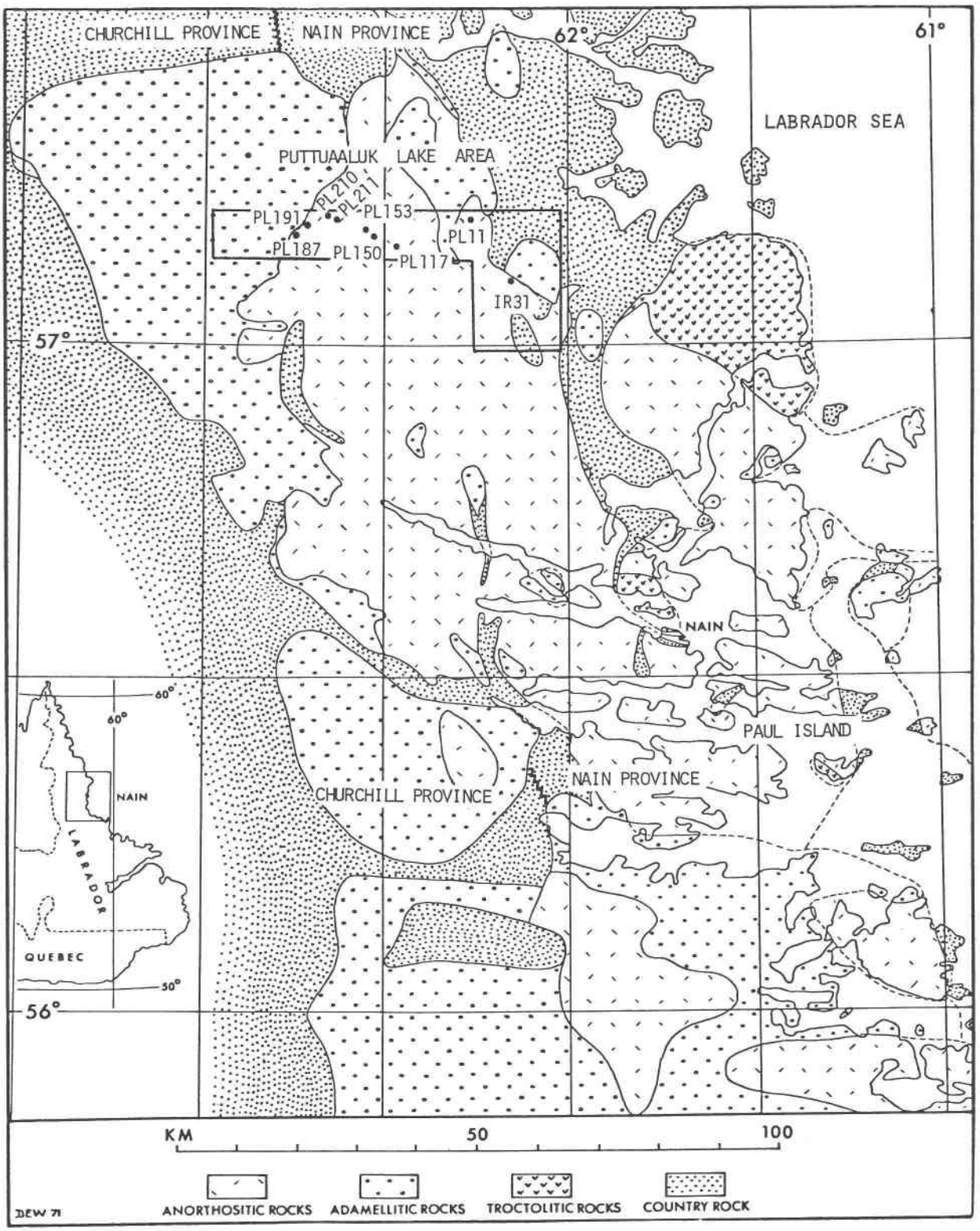

Fig. 1. Geologic map of Nain complex showing boundaries of Puttuaaluk Lake area and locations of pyroxene specimens. See App. 1 for specimen descriptions. Map compiled by D. de Waard based primarily on field work of E. P. Wheeler II.

complex, Labrador, specifically from the Puttuaaluk Lake area (Ranson, 1978, 1979, 1981). This area transects the Helikian Nain complex, which consists of greater than 10 000 km^2 of anorthositic rocks and a nearly equal area of intermediate to granitic rocks (Fig. 1). The anorthositic, intermediate, and granitic rocks of the Nain complex are unmetamorphosed, and all of the investigated pyroxenes are the products of slow cooling from their temperatures of crystallization at pressures of 3 to 4 kbar (Berg, 1977, and pers. comm., 1983).

The petrography of the pyroxene-bearing rock types from the Nain complex is briefly discussed in the next section. Detailed descriptions of the nine specimens considered in this report are found in Appendix 1.

Petrography

Seven of the nine pyroxene specimens investigated are from anorthositic rocks; the remaining two samples are from granitic and intermediate rock types. Anorthositic rocks have been divided by Ranson (1979, 1981) into three mappable units: anorthosite, leuconorite, and oxide-rich anorthosite. Pyroxenes occurring in these three anorthositic units are different in composition, grain size, habit, and in textural relationship to plagioclase. The anorthosite unit has a color index less than 10 and contains predominantly Ca-rich pyroxenes, which occur as fine-grained, anhedral, interstitial phases. The leuconorite has a color index averaging between 10 and 30 and carries Ca-poor pyroxenes as the dominant mafic mineral. Ca-poor pyroxenes are primary orthopyroxene in leuconorites of magnesian composition and inverted pigeonite in more Fe-rich leuconorites. Most pyroxenes in leuconorites occur as medium-grained, subhedral to euhedral phases, suggesting simultaneous crystallization of plagioclase and pyroxene (Ranson, 1981). The oxide-rich anorthosite, with color index between 5 and 30, is distinguished by 5 to 15% Fe-Ti oxide minerals in addition to chiefly Ca-poor pyroxenes. For all of the oxide-rich anorthosite specimens studied, the Ca-poor pyroxene is inverted pigeonite rather than primary orthopyroxene.

Granitic and intermediate rocks in the Puttuaaluk Lake area include granite, quartz monzonite, monzonite, quartz monzodiorite and diorite, all of which show strong Fe enrichment. Ca-rich pyroxenes may be present in all of the above rocks, whereas Ca-poor pyroxenes (inverted pigeonites) are restricted to quartz monzodiorite, monzodiorite, and diorite. In the more Si-rich rocks approaching granite in composition, Ca-rich pyroxenes are reduced in abundance, and Fe-rich amphibole is the major mafic mineral. Fayalitic olivine is commonly associated with Ca-rich pyroxenes but rarely coexists with inverted pigeonites.

Optical properties and composition of pyroxenes

Determinative methods

Measurement of n_γ of Ca-rich and Ca-poor pyroxenes was made on crushed grains in oil-immersion mounts. Some specimens contained only minor or interstitial Ca-rich pyroxene that could be analyzed by electron microprobe in thin section but did not appear in grain mounts, and hence n_γ was not obtained for these pyroxenes. For reasons cited in Jaffe et al. (1975), n_γ rather than n_β was measured for Ca-rich pyroxenes.

Chemical analyses of pyroxenes were obtained by electron microprobe. Microprobe analyses were performed at 15-kV accelerating potential and an aperture current of 0.03 μA on an automated electron microprobe at either the University of Massachusetts (ETEC autoprobe) or the Massachusetts Institute of Technology (MAC 500 probe). Standards used to report element weight percent values were as follows: synthetic pyroxene ($Di_{65}Jd_{35}$) for Na and Si (source: F. R. Boyd, Geophysical Laboratory); synthetic Cr-rich diopside for Mg, Si, and Ca (source: J. F. Schairer's lab, Geophysical Laboratory); chromite for Al and Cr (source: Stillwater complex, 52-NL-11); sanidine for Si and K (source: R. V. Dietrich, Leilen Kopf, Germany); Mn-bearing ilmenite for Ti, Mn, Fe (source: USNM sample 96189). Matrix corrections were made following the procedure of Bence and Albee (1968), using the alpha factors of Albee and Ray (1970). An electron-beam diameter of 0.5–1.0 μm was used for analyzing broad exsolution lamellae and for the host pyroxene in between lamellae. Where exsolution lamellae were too fine to be resolved with the electron beam, a broader beam with a diameter of 10–12 μm was used. Bulk compositions for exsolved pyroxenes were calculated by first determining the proportion of host to lamellae from enlarged photomicrographs of pyroxene crystals. Paper tracings of host and lamellar portions of single grains were cut apart and weighed to obtain the host : lamellae volumetric ratio. Probe analyses of host and lamellae were then used in the indicated proportions to determine the bulk compositions. The compositions taken for host and lamellar phases are averages of 10 to 30 spot analyses.

Results

Exsolution type, n_γ and composition of Ca-poor and Ca-rich pyroxenes are posted in Table 1. The n_γ for augite is listed for only two samples in Table 1 for the reason cited above (see App. 1 for complete sample descriptions). Complete chemical analyses of hosts, lamellae, and bulk grains with formulae for both Ca-poor and Ca-rich pyroxenes are tabulated in Table 2. Figure 2 shows the variation of n_γ and the atomic ratio $100(Fe_t + Mn)/(Mg + Fe_t + Mn)$ for orthopyroxenes and inverted pigeonites. Scatter about the visually fit curve and the least-squares linear best fit probably reflects the difficulty of obtaining accurate analyses of these highly exsolved host pyroxenes. Despite the scatter, the curves do not differ greatly from those obtained by Jaffe et al. (1975) for metamorphic orthopyroxenes.

Even with the difficulties involved in obtaining meaningful analyses of finely exsolved pyroxenes, most of the analyses posted in Table 2 have cation totals of 4.00 ± 0.02 based on six oxygens. Nonquadrilateral components,

Table 1. Exsolution type, n_γ, and composition of pyroxenes from the Puttuaaluk Lake area

Sample	Exsolution type*	Opx		Aug	
		n_γ	Comp.**	n_γ	Comp.**
PL-11	1	1.741	59.4	1.7375	46
PL-150	1	1.7085	34.1	—	24
IR-31	2?	—	53.9	—	—
PL-117	2	1.7373	50.3	1.723	38
PL-211	2	1.7426	57	—	—
PL-153	2	1.722	45.9	—	—
PL-210	3	1.748	62.9	—	—
PL-187	3	1.765	78.7	—	69
PL-191	3	1.763	77.6	—	—

* Refers to the three types of exsolution observed in Ca-poor pyroxenes; see text for descriptions.
** Composition: $100(Fe_t + Mn)/(Mg + Fe_t + Mn)$ for host.

including Al_2O_3, TiO_2, K_2O, Na_2O, MnO, and Cr_2O_3, are slight in amount, usually summing to less than 1.50wt%. For all microprobe analyses, total Fe was determined and reported as FeO. Wo, En, and Fs contents, as indicated in Table 2, were calculated according to the method of Lindsley and Andersen (1983) for application of their pyroxene geothermometer.

Exsolution in Ca-poor pyroxenes

Morphology

Inasmuch as exsolution features in Nain augites are nearly identical to those described elsewhere (Robinson et al., 1977; Rietmeijer, 1979; Huntington, 1980), these pyroxenes will receive only brief mention. The major description and discussion will be devoted to the exsolution in Ca-poor pyroxenes. Ca-poor pyroxenes from the Puttuaaluk Lake area have been grouped into three types on the basis of optically observed exsolution features (Ranson, 1978). Type 1 pyroxenes are primary magnesian [$Fe_t + Mn)/(Mg + Fe_t + Mn) < 60$] orthopyroxenes and lack exsolution or more typically contain only fine (100) augite lamellae (Fig. 3). This type of exsolution, described by Hess and Phillips (1940) as the Bushveld type, is believed to have formed upon cooling of orthopyroxene precipitated directly from the liquid. The magnesian compositions are in accord with the findings of Poldervaart and Hess (1951) and Wager and Brown (1967), who showed that for magnesium compositions, crystallization takes place within the orthopyroxene stability field, whereas for Fe-rich compositions, crystallization takes place within the stability field of monoclinic pyroxene. Many factors, in addition to Fe enrichment, play a role in determining whether orthopyroxene or pigeonite is the pyroxene forming on the liquidus. Some of these factors will be addressed in the discussion section.

The second category of Ca-poor pyroxenes, type 2, consists of pigeonites that have exsolved augite and undergone transformation from the $C2/c$ or $P2_1/c$ structure of pigeonite to the *Pbca* structure of orthopyroxene. Exsolved pyroxene in type 2 pyroxenes takes the form of irregular lamellae, granules, and blebs of augite 40–100 μm in width. Blebs of augite are variable in size and shape and show no preferred crystallographic orientation relative to the host. Irregular lamellae are generally aligned subparallel and usually go to extinction simultaneously in cross-polarized light, indicating like crystallographic orientation with respect to each other. Exsolved augite may itself contain finely exsolved pigeonite lamellae of "100" and "001" orientation. Some type 2 pyroxenes contain fine (100) augite lamellae more characteristic of type 1 pyroxene. Granules of augite at the margins of type 2 pyroxenes probably have resulted from granule exsolution. Photomicrographs of pyroxene crystals illustrating type 2 exsolution are shown in Figure 4.

Type 3 pyroxenes contain the most interesting and complicated exsolution features, some of which have not been previously described to the writer's knowledge. Like the type 2 pyroxenes, type 3 pyroxenes are inverted pigeonites, and both types belong to the category referred to as Stillwater-type pyroxenes by Hess (1941).

The most distinctive features of the type 3 pyroxenes are the broad (40–50 μm in width), regularly spaced augite lamellae oriented parallel to an irrational plane near (001) of the host inverted pigeonite. Because these lamellae are analogous to the broad "001" (Pig I) lamellae in host augite described by Robinson et al. (1971, 1977), they are classed here as Aug I. These broad "001" augite lamellae (Aug I) are typically continuous across entire crystals and slightly curved at the ends (Fig. 5a). Robinson et al. (1977) have pointed out that curved lamellae record changing lattice parameters associated with changing environmental conditions of pressure, temperature, and composition. Up to two sets of "001" pigeonite lamellae have in turn been observed enclosed in the coarse Aug I lamelle, a broad set (Pig II), 0.5–1.0 μm in width, and a finer set (Pig III) 0.05–0.1 μm in width, at a slight angle to the broader set (Fig. 5b). These are the Pig II and Pig III lamellae of Robinson et al. (1977). Coarse Pig I lamellae (thickness 5–12 μm) of Robinson et al. (1977) were not observed. Both Pig II and Pig III lamellae are short and discontinuous across enclosing augite lamellae. Pig III lamellae are more numerous than Pig II lamellae and are concentrated away from them (Fig. 5b). In addition to the broad set of augite lamellae oriented on "001" (Aug I), a second set of augite lamellae occurs with a "100" orientation. Aug "100" lamellae are 5–10 μm in width and contact broader Aug I lamellae but do not penetrate them. Aug "100" lamellae are straight and typically continuous, although they may be confined to certain portions of an individual grain, as seen in Figure 6. Also, Aug "100" lamellae are most abundant in portions of crystals where Aug I lamellae are absent (upper half of Fig. 6). Fine (≤ 1 μm) (100) augite lamellae of the Bushveld-type may be present in the orthopyroxene host and represent low-temperature exsolution after the original pigeonite had inverted to orthopyroxene.

Some type 3 pyroxenes, notably those found in PL-191 (see App. 1), contain a second, much narrower set of "001" augite lamellae (Aug II). The Aug II lamellae are rather uncommon, are discontinuous across the host crystal, and

Table 2. Electron-microprobe analyses and recalculated bulk compositions of coexisting pyroxenes with formulae based on six oxygens

	PL-11		PL-150		IR-31			PL-117-A			PL-117-B			PL-211-A		
	Ca-poor pyroxene	Ca-rich pyroxene	Ca-poor pyroxene	Ca-rich pyroxene	Ca-poor host	Augite granules	Bulk comp.	Ca-poor host	Augite blebs	Bulk comp.	Ca-rich host	Pig lamellae	Bulk comp.	Ca-poor host	Augite lamellae	Bulk comp.
SiO_2	50.89*	52.02*	53.34*	52.13*	50.59*	51.03*	50.64*	51.03*	52.61*	51.23*	51.45	51.39	51.45*	47.96*	52.18*	48.75*
Al_2O_3	0.62	1.40	0.64	1.13	0.96	1.78	1.05	0.53	1.05	0.60	1.30	0.58	1.25	0.50	0.99	0.59
TiO_2	0.16	0.25	0.23	0.41	0.12	0.35	0.14	0.19	0.21	0.19	0.39	0.18	0.38	0.17	0.30	0.19
Cr_2O_3	0.02	0.03	0.02	0.15	0.05	0.03	0.05	0.07	0.04	0.06	0.08	0.04	0.08	0.03	0.04	0.03
FeO	33.89	14.74	21.47	8.09	31.00	12.40	29.03	29.92	12.27	27.63	12.98	30.11	14.11	34.84	15.02	31.15
MnO	0.79	0.43	0.36	0.17	0.85	0.38	0.80	0.48	0.22	0.45	0.19	0.52	0.21	0.54	0.28	0.49
MgO	13.33	10.13	23.66	15.03	15.30	11.70	14.92	16.86	12.54	16.30	12.23	17.40	12.57	15.06	11.23	14.35
CaO	0.80	20.99	1.10	23.22	0.74	20.71	2.85	1.27	21.73	3.92	20.80	0.74	19.48	1.07	20.71	4.73
Na_2O	0.00	0.07	0.01	0.18	0.00	0.27	0.03	0.02	0.18	0.04	0.13	0.02	0.12	0.01	0.14	0.03
K_2O	0.00	0.00	0.00	0.00	0.00	0.00	0.00	0.00	0.00	0.00	0.00	0.00	0.00	0.00	0.00	0.00
Total	100.50	100.07	100.83	100.51	99.61	98.65	99.51	100.37	100.85	100.42	99.55	100.98	99.65	100.18	100.89	100.31
Si	1.996	1.985	1.964	1.937	1.979	1.958	1.977	1.971	1.970	1.971	1.958	1.969	1.959	1.914	1.975	1.925
Al	0.004	0.015	0.028	0.049	0.021	0.042	0.023	0.023	0.030	0.024	0.042	0.025	0.041	0.023	0.025	0.023
Al	0.025	0.048	0.000	0.000	0.023	0.039	0.025	0.000	0.016	0.002	0.016	0.000	0.015	0.000	0.019	0.004
Ti	0.005	0.008	0.006	0.011	0.004	0.010	0.005	0.004	0.005	0.004	0.010	0.004	0.009	0.005	0.009	0.006
Cr	0.000	0.001	0.001	0.004	0.002	0.001	0.002	0.001	0.001	0.001	0.002	0.000	0.002	0.001	0.001	0.001
Fe	1.113	0.471	0.662	0.252	1.015	0.398	0.950	0.965	0.383	0.889	0.412	0.965	0.450	1.164	0.476	1.036
Mn	0.026	0.011	0.011	0.005	0.028	0.012	0.026	0.015	0.006	0.014	0.005	0.017	0.006	0.018	0.009	0.016
Mg	0.780	0.577	1.299	0.833	0.893	0.669	0.869	0.970	0.700	0.935	0.693	0.994	0.713	0.896	0.634	0.847
Ca	0.032	0.859	0.043	0.925	0.031	0.852	0.118	0.052	0.871	0.158	0.848	0.030	0.794	0.046	0.840	0.194
Na	0.000	0.000	0.000	0.013	0.000	0.020	0.002	0.001	0.012	0.002	0.009	0.001	0.008	0.001	0.010	0.003
K	0.000	0.001	0.000	0.000	0.000	0.000	0.000	0.000	0.000	0.000	0.000	0.000	0.000	0.000	0.000	0.000
Total	3.972	3.976	4.014	4.029	3.996	4.001	3.997	4.003	3.995	4.000	3.995	4.006	3.997	4.068	3.998	4.035
Wo	1.7	40.5	2.2	44.9	1.6	41.6	7.8	2.6	43.1	8.9	43.4	1.5	38.9	2.2	41.5	6.1
En	40.5	32.8	65.5	44.4	46.1	36.7	44.1	49.3	37.3	47.2	35.5	49.9	37.8	42.8	33.4	42.6
Fs	57.8	26.7	32.3	10.8	52.4	21.7	48.1	48.0	19.6	43.9	21.1	48.5	23.2	55.0	25.1	51.3
% of grain	100.00	100.00	100.00	100.00	89.43	10.57	100.00	87.07	12.93	100.00	93.43	6.57	100.00	81.36	18.64	100.00

Table 2—*Continued*

	PL-153			PL-210-A			PL-187-A			PL-187-B			PL-191-A			PL-191-B		
	Ca-poor host	Augite blebs	Bulk comp.	Ca-poor host	Augite lamel-lae	Bulk comp.	Ca-poor host	Augite lamel-lae	Bulk comp.	Ca-rich host	Pig lamel-lae	Bulk comp.	Ca-poor host	Augite lamel-lae	Bulk comp.	Ca-rich host	Pig lamel-lae	Bulk comp.
SiO_2	50.44*	50.42*	50.43*	48.25*	48.40*	48.28*	47.73*	49.75*	48.25*	49.55	48.14	49.23*	46.21*	49.33*	47.11*	49.17	48.79	49.02*
Al_2O_3	0.82	1.33	0.91	0.39	0.88	0.50	0.29	0.75	0.41	0.86	0.34	0.74	0.30	0.91	0.47	1.12	0.46	0.86
TiO_2	0.24	0.24	0.24	0.14	0.21	0.16	0.15	0.19	0.16	0.17	0.21	0.18	0.23	0.59	0.33	0.40	0.28	0.35
Cr_2O_3	0.01	0.02	0.01	0.00	0.01	0.00	0.00	0.01	0.00	0.02	0.00	0.02	0.01	0.00	0.01	0.05	0.06	0.05
FeO	28.67	11.41	25.75	36.26	17.89	32.10	43.25	24.05	38.33	23.13	42.91	27.66	42.28	23.45	36.85	24.51	40.21	30.64
MnO	0.51	0.24	0.46	0.61	0.33	0.55	0.84	0.36	0.72	0.44	0.77	0.52	0.78	0.31	0.65	0.36	0.65	0.47
MgO	19.34	13.92	18.42	12.18	10.19	11.72	6.68	6.02	6.51	6.06	6.73	6.21	6.98	5.90	6.67	6.18	6.80	6.42
CaO	0.98	22.59	4.64	2.93	21.77	7.19	1.31	19.14	5.88	19.49	1.57	15.38	3.47	20.10	8.26	18.57	4.23	12.97
Na_2O	0.00	0.21	0.04	0.00	0.09	0.02	0.01	0.20	0.06	0.24	0.02	0.19	0.00	0.13	0.04	0.18	0.08	0.14
K_2O	0.00	0.00	0.00	0.00	0.00	0.00	0.00	0.00	0.00	0.00	0.00	0.00	0.00	0.00	0.00	0.00	0.00	0.00
Total	101.01	100.38	100.90	100.76	99.77	100.54	100.27	100.46	100.32	99.96	100.68	100.13	100.26	100.72	100.39	100.52	101.56	100.92
Si	1.927	1.908	1.924	1.935	1.903	1.928	1.981	1.974	1.979	1.972	1.984	1.975	1.932	1.953	1.938	1.951	1.979	1.962
Al	0.037	0.059	0.041	0.018	0.041	0.023	0.013	0.026	0.016	0.028	0.016	0.025	0.015	0.043	0.023	0.049	0.021	0.038
Al	0.000	0.000	0.000	0.000	0.000	0.000	0.000	0.008	0.002	0.012	0.000	0.009	0.000	0.000	0.000	0.003	0.000	0.002
Ti	0.007	0.007	0.007	0.004	0.006	0.004	0.003	0.004	0.003	0.004	0.006	0.004	0.007	0.018	0.010	0.011	0.008	0.004
Cr	0.000	0.001	0.000	0.000	0.000	0.000	0.000	0.000	0.000	0.000	0.000	0.000	0.000	0.000	0.000	0.001	0.001	0.001
Fe	0.917	0.361	0.823	1.217	0.589	1.075	1.500	0.798	1.320	0.769	1.478	0.932	1.480	0.777	1.277	0.813	1.364	1.029
Mn	0.017	0.008	0.016	0.021	0.011	0.019	0.029	0.011	0.024	0.014	0.026	0.017	0.027	0.010	0.022	0.011	0.021	0.015
Mg	1.102	0.786	1.049	0.729	0.598	0.699	0.413	0.355	0.398	0.358	0.412	0.370	0.435	0.348	0.410	0.364	0.410	0.382
Ca	0.040	0.917	0.188	0.126	0.918	0.305	0.057	0.813	0.251	0.830	0.069	0.655	0.156	0.835	0.352	0.790	0.183	0.553
Na	0.000	0.015	0.003	0.000	0.007	0.002	0.000	0.014	0.004	0.017	0.001	0.013	0.000	0.010	0.003	0.013	0.006	0.010
K	0.000	0.000	0.000	0.000	0.000	0.000	0.000	0.000	0.000	0.000	0.000	0.000	0.000	0.000	0.000	0.000	0.000	0.000
Total	4.047	4.062	4.051	4.050	4.073	4.055	3.997	4.003	3.999	4.004	3.991	4.000	4.052	4.012	4.040	4.006	3.993	3.996
Wo	2.0	44.4	6.7	6.1	44.8	11.5	2.9	40.5	14.3	42.4	3.5	32.6	7.5	41.7	16.0	40.2	9.4	26.7
En	54.1	40.2	53.1	35.4	28.7	35.2	21.0	18.7	20.0	18.3	21.0	18.9	21.0	18.4	20.5	18.5	20.9	19.8
Fs	43.9	15.5	40.2	58.5	26.5	53.3	76.1	40.8	65.7	39.3	75.5	48.0	71.5	39.9	63.5	41.3	69.7	53.5
% of grain	83.07	16.93	100.00	77.37	22.63	100.00	74.39	25.61	100.00	77.08	22.92	100.00	71.17	28.83	100.00	60.95	39.05	100.00

* Molecular percent calculated according to the procedure of Lindsley and Andersen (1983) for application of pyroxene geothermometer.

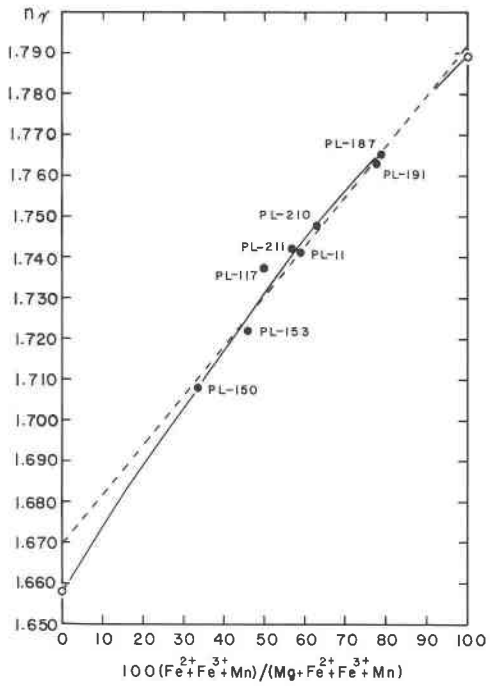

Fig. 2. The ratio 100 (Fe^{2+} + Fe^{3+} + Mn)/(Mg + Fe^{2+} + Fe^{3+} + Mn) versus n_γ for Ca-poor pyroxenes from Puttuaaluk Lake area. Dashed line is result of linear regression analysis with r^2 = 0.969. The equation for this line is $n_\gamma = 0.1235[(Fe_t + Mn)/(Mg + Fe_t + Mn)] + 1.6689$. Solid curve is visually fit to the data. Open circles are indices of synthetic enstatite (1.658) and orthoferrosilite (1.789) from Stephenson et al. (1966) and Lindsley et al. (1964), respectively.

Fig. 3. Photomicrograph of type 1 (Bushveld-type) exsolution in leuconorite sample PL-150. Exsolution consists of fine (100) augite and parallel Fe-Ti oxide minerals. Scale bar is 0.10 mm.

occur midway between broad Aug I lamellae at a slightly steeper orientation (Fig. 6).

Another interesting characteristic of type 3 pyroxene is the presence of patches of pigeonite in the host regions of the crystal, which suggest that transformation of the host to orthopyroxene was not complete. Patches of pigeonite are referred to as Pig O since these remnants of original host pigeonite preceded pigeonite exsolved from broad Aug I lamellae. Pig O patches, as seen in Figure 6, appear bordered on all sides by Aug I, Aug II, and Aug "100" lamellae and are thus isolated, at least in the plane of the thin section, from the rest of the host. Aug II lamellae have not been observed penetrating pigeonite patches.

Other features characteristic of type 3 pyroxenes are numerous, fine stacking faults similar to those described by Robinson et al. (1977) in Bushveld augites containing pigeonite exsolution. These stacking faults, discernible only at high magnification, are oriented on (100) and cut through orthopyroxene host, patches of uninverted pigeonite host, and broad "001" augite lamellae (Fig. 5b). Stacking faults rotate 2–4° in a counterclockwise sense as they pass from host and pigeonite patches into broad "001" augite lamellae but have the same orientation in both the orthopyroxene and pigeonite host regions. In pyroxenes from PL-191, stacking faults are particularly numerous and appear to be accompanied by fine, parallel exsolution lamellae, probably Aug (100).

In some anorthositic specimens, notably PL-187 (see App. 1), Ca-poor and Ca-rich pyroxenes appear to be completely intergrown. In such cases, sizable patches of orthopyroxene are penetrated and bordered by coarse "001" augite lamellae. The bordering augite lamellae are not actually lamellae but extend outward to form the host portion of the augite crystal.

Discussion

Type 1 pyroxenes crystallized as orthopyroxenes below the pigeonite → orthopyroxene + augite transition temperature. Ross and Huebner (1979), through their heating experiments, have shown the dependency of the temperature of this reaction upon Fe/Mg ratio. At 1 bar they determined that the upper temperature limit for the minimum stability temperature of pigeonite varied from 1284°C at Mg/(Mg + ΣFe) = 0.92 (atomic) to 901°C at 0.04. In the same study Ross and Huebner also compared two orthopyroxenes in order to show the relationship between temperature and the Ca content of orthopyroxene involved in this reaction. A second purpose was to illustrate the interface reaction mechanism. Their orthopyroxene sample 3 ($\sim Ca_{0.012}Mg_{1.748}Fe_{0.252}Si_2O_6$), which contains lamellae of augite (orientation not given) 7 to 20 μm thick, had pigeonite first appearing in the run products heated to 1259°C. A second sample, sample 29, consists of chemically homogeneous orthopyroxene ($Ca_{0.012}Mg_{1.636}Fe_{0.352}Si_2O_6$), which contains no lamellae of augite.

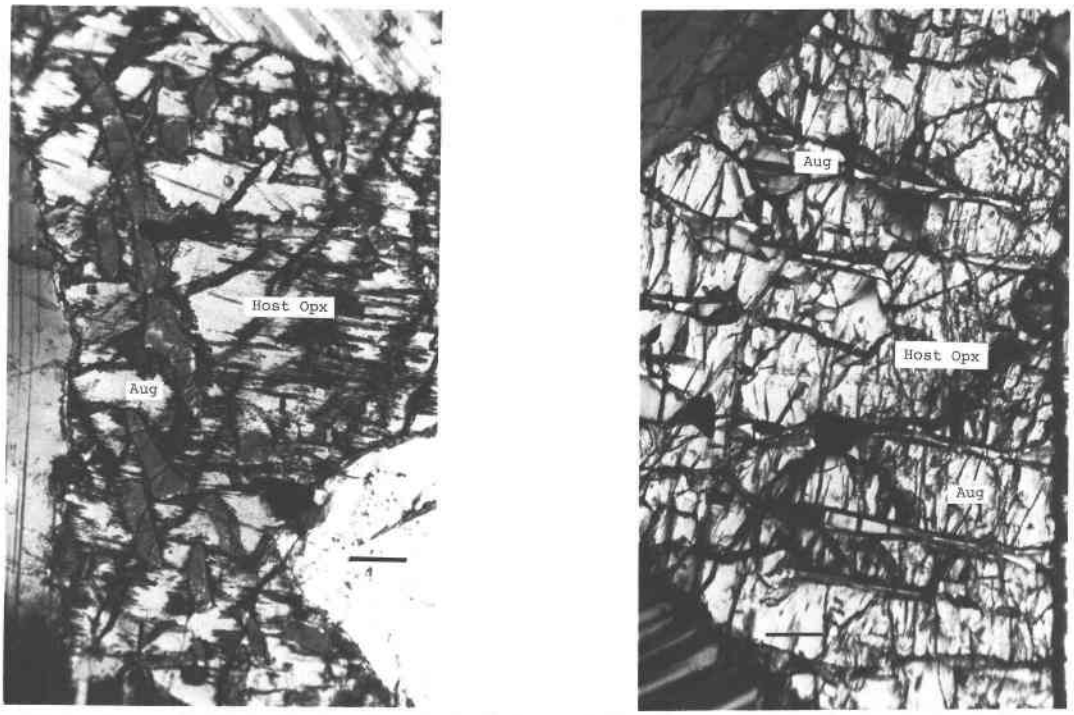

Fig. 4. Photomicrographs illustrating type 2 exsolution in inverted pigeonites. (a, left) Exsolved augite in the form of blebs and granules in sample IR-31. (b, right) Inverted pigeonite sample PL-117 with irregular exsolved augite. Scale bar is 0.10 mm.

Being less magnesian than sample 3, it was expected to form pigeonite at a lower temperature. In fact, pigeonite did not appear in the run products until 1375°C. Ross and Huebner concluded from these experiments that the first appearance of pigeonite is dependent on not just the Fe/Mg ratio but also on the local Ca content and the presence of augite lamellae, which serve as favorable nucleation sites. Results of experiments on sample 3 clearly show that orthopyroxene reacted with adjacent augite lamellae to form pigeonite + melt.

Other factors may play a role in determining whether orthopyroxene or pigeonite is the pyroxene forming on the liquidus. Huebner and Turnock (1980) have shown in a series of melting experiments on synthetic and natural pyroxenes that minor elements, especially Al and Ti, are important in determining the position of the solidus. Using synthetic compositions in the system $CaSiO_3$-$MgSiO_3$-$FeSiO_3$, their experiments show that the solidus at constant Wo = 15% lies at temperatures above the pigeonite → orthopyroxene + augite transition, thus allowing Fe-free pigeonite to exist. In contrast, their results in melting experiments on natural pyroxenes reveal that the solidus occurs at lower temperatures than for the pure system and below the pigeonite → orthopyroxene + augite transition for magnesian compositions [Fe/(Fe + Mg) < 0.20] (see their Fig. 12).

Pressure also affects the pigeonite → orthopyroxene + augite relationship, producing an increase in reaction temperature of about 7 deg/kbar (Brown, 1968). However, pressure differences among the Nain pyroxenes are probably slight.

Thus it is to be expected that differences in minor-element concentrations and whole-rock chemistry will result in shifts in the stability fields of pigeonite and orthopyroxene. In general, the more magnesian pyroxenes would be expected to crystallize as orthopyroxene, but a review of Tables 1 and 2 reveals that this is not always the case. It should be noted that of the type 1 pyroxenes, only sample PL-11 was saturated with augite as orthopyroxene crystallized. All type 2 pyroxenes contain minor augite, but not one of them appears to have been saturated with augite. Finally, only sample PL-187 of the type 3 pyroxenes was saturated with augite.

As expected in primary orthopyroxene hosts, exsolution of augite as lamellae is restricted to the (100) plane. For these two structurally distinct pyroxenes, (100) is not a plane of exact fit, but it does offer the best dimensional match (Robinson, 1980). The two possible processes responsible for the initiation of exsolution in pyroxenes are spinodal decomposition and nucleation and growth. In this case the spinodal mechanism can be ruled out because of the difference in structure of the two pyroxenes (Champness and Lorimer, 1976).

Type 2 and type 3 pyroxenes are similar to one another in that both crystallized as pigeonite, exsolved augite, and then the host portion, or most of it, underwent transition to orthopyroxene. The major differences between the two pyroxene types are the form and orientation of the exsolved augite, which most likely reflect the cooling history and composition of the original pigeonite. Further explanation of these differences will be considered later in the report when mechanisms of exsolution are discussed. Compar-

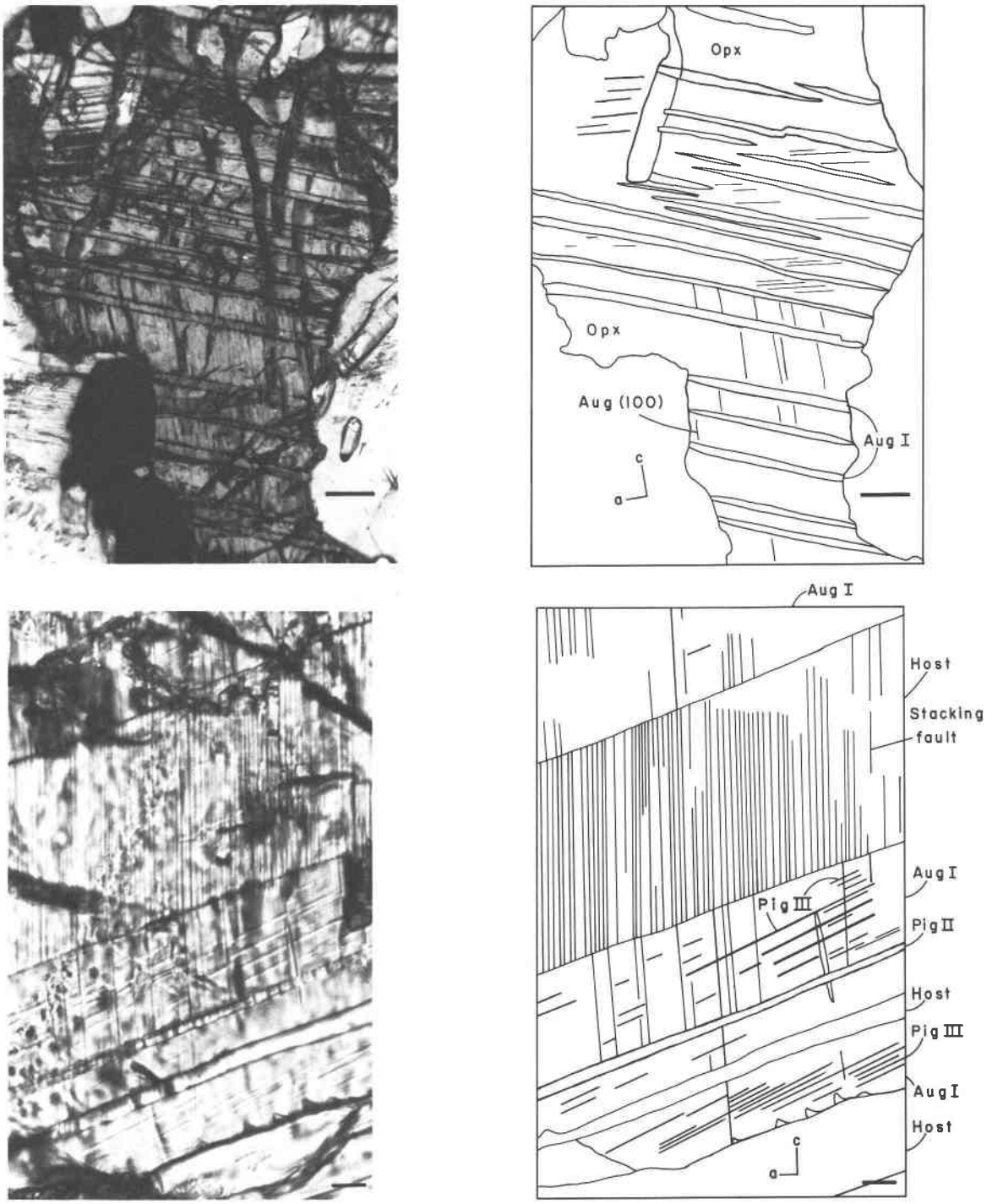

Fig. 5. Photomicrographs and tracings of exsolved pyroxenes in type 3 Nain pyroxenes. (a, upper) Broad, regularly spaced "001" augite lamellae (Aug I) in PL-210. Scale bar is 0.10 mm. (b, lower) Detail of broad "001" augite lamellae (Aug I) in PL-191 showing fine pigeonite lamellae, Pig II and Pig III, and stacking faults that rotate counter-clockwise as they pass through Aug 1 lamellae (see text for details). Scale bar is 10 μm.

ison of original pigeonite compositions (Table 2) shows that type 3 pyroxenes are enriched both in Fs and Wo content relative to type 2 pyroxenes. Type 3 pyroxenes occur in rocks that appear to be the final or extreme differentiate of the anorthosite-leuconorite suite, whereas type 2 pyroxenes occur in less differentiated, more typical rocks of the suite (see App. 1). The regular lamellae, both "001" (Aug I and Aug II) and "100" (Aug "100"), represent the

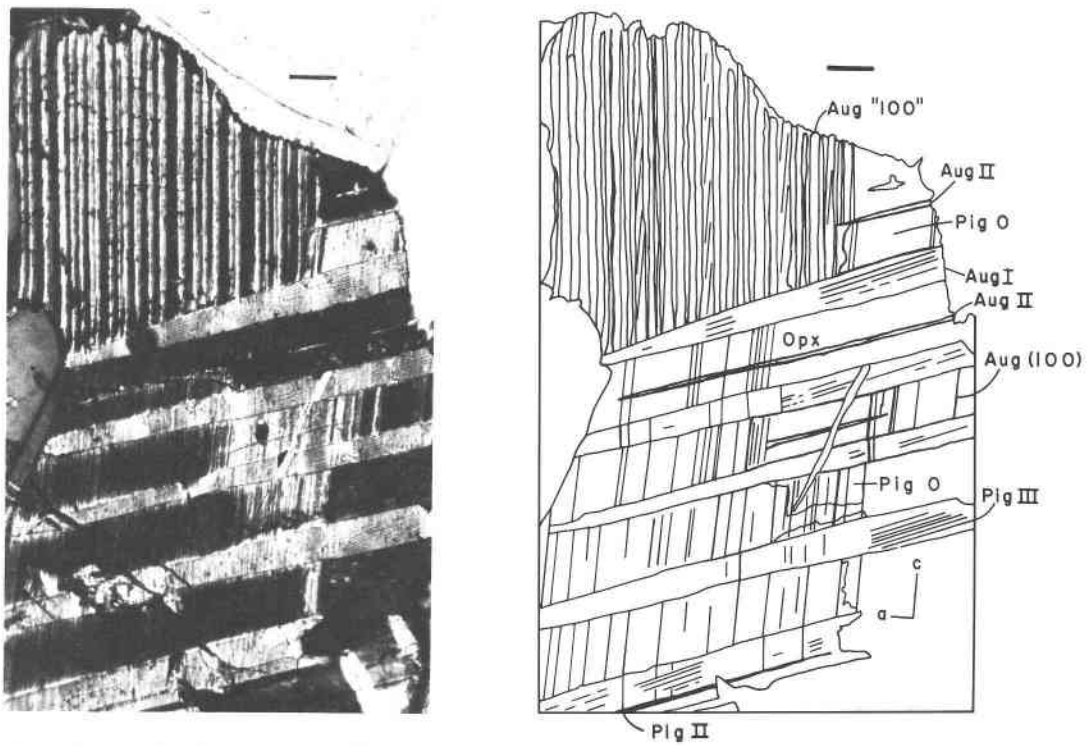

Fig. 6. Photomicrograph and tracing of type 3 pyroxene PL-191 showing four generations of augite exsolution: broad "001" Aug I, fine "001" Aug II, Aug "100", and Aug (100). Note the light patches of pigeonite host (Pig O) constrained by augite lamellae, which failed to invert. Aug I lamellae have exsolved two sets of pigeonite lamellae, Pig II and the finer Pig III. The host orthopyroxene is at extinction. Fine straight lines parallel to (100) are stacking faults. Scale bar is 50 μm.

two planes of exact dimensional fit, one near (001) and the other near (100), in accordance with the exact phase boundary theory (Bollman and Nissen, 1968; Jaffe et al., 1975). The single most important factor determining the orientation of "001" lamellae is the misfit of the a dimension of pigeonite and augite. Similarly the orientation of "100" lamellae is a function of the misfit of the c dimension of pigeonite and augite. In the same manner the "001" and "100" orientations of pigeonite lamellae in exsolved augite of type 2 or type 3 pyroxenes may be explained. Although augite exsolution from pigeonite in type 2 pyroxenes was irregular, pigeonite exsolution achieved the "exact dimensional fit" described above, presumably because the pigeonite exsolved from the augite lamellae at a later time and at a lower temperature.

A further difference between type 2 and type 3 pyroxenes is that in most type 2 pyroxenes stacking faults are not present or are at least not visible with the optical microscope. The reason for this is not clear, especially since both pyroxene types are inverted pigeonites and stacking faults appear to figure prominently in the pigeonite to orthopyroxene transition, as discussed below. Without the benefit of electron microscopy, the absence of stacking faults in most type 2 pyroxenes is open to speculation. The following discussion assumes their presence in all inverted pigeonites.

Robinson et al. (1977) explained stacking faults in Bushveld augites as minute normal faults developed on (100) that relieve the strain produced by the unequal change of unit-cell parameters by host augite and pigeonite. The unequal change in the unit cell is brought on by the $C2/c \rightleftharpoons P2_1/c$ transition and means that the unit cell of pigeonite changes more rapidly than that of augite during cooling, and as a result the pigeonite lamellae are severely strained. The faulting allows the crystallographic angle β of a pigeonite lamella to equilibrate to lower temperatures for each small, faulted lamella segment, thereby reducing the strain for the entire lamella. Robinson and coworkers also pointed out that faults are most abundant in the thickest pigeonite lamellae, which follows since fault density should correlate with the amount of lattice change a pigeonite lamella has undergone. Hence high-temperature, early-formed, thick lamellae with a long cooling history were found to contain a greater density of stacking faults by these authors than thinner lamellae formed at a lower temperature.

An analogous situation seems to be present in Nain type 3 pyroxenes, but with pigeonite being the host and augite the exsolved guest. Like the Bushveld augites, the Nain pigeonites and their exsolved augite lamellae must have experienced strain as cooling occurred and the rate of change of the pigeonite and augite unit cells differed. Strain was again relieved by small-scale faulting on (100). Unlike the Bushveld augites, stacking faults are found not

only in the lamellae, but also in the host regions. For the host, faults have the same orientation regardless of whether the host is pigeonite or orthopyroxene.

It seems likely that the faults are the mechanism by which the $P2_1/c \rightarrow Pbca$ transition occurs for the host. Robinson et al. (1977) attributed the production of a strip of orthopyroxene in Bushveld augite to stacking faults, and Coe and Kirby (1975) reported that shear on (100) produces the transformation of orthoenstatite to clinoenstatite. However, their experiments show that the transformation is mechanically reversible. Champness and Copley (1976) stated that the (100) stacking faults in pigeonite lamellae exsolved from augite may initiate the inversion reaction. Faults preferentially nucleate at growth ledges at interphase boundaries, according to Champness and Copley, because these are the regions of highest strain energy and some of this strain energy can be used to counteract the activation barrier opposing fault formation. These same authors cited evidence by Morimoto and Koto (1969) that the orthoenstatite structure could be produced from that of clinoenstatite by twinning of every unit cell on (100), and they stated further that although clinoenstatite and pigeonite are slightly different structurally, a (100), 1/6 [001] fault is a possible means of generating orthopyroxene from pigeonite.

In Nain pyroxenes, patches of uninverted pigeonite may still contain stacking faults, but these patches are always surrounded by "001" and "100" augite lamellae (Fig. 6) and are thereby isolated from the rest of the host. They were apparently constrained so that the change from monoclinic to orthohombic lattice could not occur completely in these areas, despite the presence of stacking faults. Smith (1974) also observed uninverted pigeonite bounded by augite lamellae in orthopyroxene from adamellite of the Nain complex (Smith's Fig. 3D). He cited the persistence of pigeonite as evidence that it was difficult for new phases to nucleate within these Nain pyroxenes.

The counterclockwise rotation or bending of (100) stacking faults in Nain pyroxenes as they pass from orthopyroxene host to "001" augite lamellae is analogous to the bending of orthopyroxene lamellae described by Robinson et al. (1977) for Bushveld augites. In that case (100) orthopyroxene lamellae bend as they pass through "001" pigeonite lamellae in order to become parallel to (100) of the lamellae. In the present example, stacking faults bend as they enter augite lamellae in order to become parallel to (100) of the augite.

Champness and Lorimer (1976) and Buseck et al. (1980) have very thoroughly reviewed the mechanisms for exsolution in silicates in general and in pyroxenes in particular, and the reader is referred to these discussions. Basically these authors have distinguished between two processes whereby exsolution may occur: (1) nucleation and growth and (2) spinodal decomposition. Buseck and co-workers pointed out that the later stages of spinodal decomposition eventually lead to exsolution features similar to those produced by nucleation and growth. Verification of spinodal decomposition involves the observation of the change of amplitude and wavelength of the compositional modulations over an interval of time and requires sophisticated small-angle X-ray scattering experiments. The observation of periodic compositional modulation of a coherent lattice by electron observation may also serve as evidence for spinodal decomposition. In its initial stages, spinodal decomposition is characterized by coherent modulations as shown in Figures 9 and 15b of Champness and Lorimer (1976). Textures of this nature have not been observed in Nain pyroxenes, although it is likely that exsolution has proceeded beyond the initial stages where such textures would be visible. In addition, judging from time-temperature-transformation (TTT) diagrams in Champness and Lorimer (1976, Fig. 7) and Buseck et al. (1980, Fig. 20), spinodal decomposition requires rapid cooling rates more appropriate to a volcanic or hypabyssal environment rather than the plutonic environment of the Nain complex where cooling was demonstrably slow. The requirement of rapid cooling is especially true for pigeonites, which are usually far from the crest of the solvus and hence are well below the temperatures for both pigeonite "inversion" and binodal exsolution before they enter the spinodal region (Lindsley, pers. comm., 1985). For these reasons, exsolution in Nain pyroxenes most likely proceeded by a mechanism of nucleation and growth.

Nucleation can be either a heterogeneous or a homogeneous process, and the textures and microstructures observed for Nain pyroxenes suggest that both processes operated. The specimens categorized as type 2 pyroxenes have irregular exsolution, and it is suggested that heterogeneous nucleation occurred at a pre-existing defect such as a dislocation in the structure, a grain or subgrain boundary where strain or surface energy is reduced. In contrast, type 3 pyroxenes display regularly spaced, quite uniform exsolution features suggestive of homogeneous nucleation. This process implies that the original pigeonite host reached a point in its cooling history where it was supersaturated with augite components, that compositional fluctuations grew to critical size (see Buseck et al., 1980, Fig. 15), and that nucleation occurred uniformly throughout the crystal. Another possibility for type 3 pyroxenes, discussed by Yund and McCallister (1970), is that of discontinuous or cellular precipitation. In discontinuous precipitation, a duplex cell consisting of the equilibrium composition of the host and a new phase, nucleates and grows from the supersaturated matrix with the incoherent interface advancing into fresh matrix. This type of grain boundary diffusion is described as being many orders of magnitude faster than volume diffusion, and so this mechanism can produce a rapid exsolution rate as compared to growth of nuclei of a new phase—for example, augite—by long-range volume diffusion (Yund and McCallister, 1970). Operation of this mechanism has never been proven for pyroxenes (Yund, pers. comm., 1986), but it is an important exsolution mechanism in alloy systems in which textural relations are very similar to those in pyroxenes.

Again with reference to the TTT diagrams of Champness and Lorimer (1976) and Buseck et al. (1980), het-

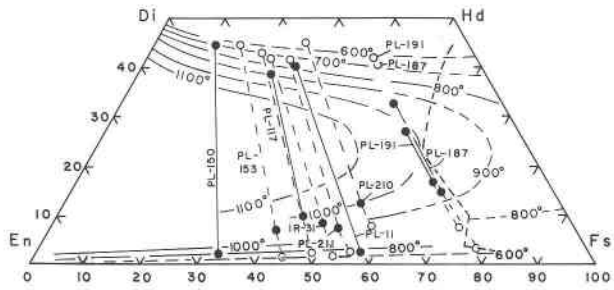

Fig. 7. Pyroxene compositions from the Puttuaaluk Lake area, Labrador, taken from Table 2. Temperature contours and plotting procedure are from Lindsley and Andersen (1983). Solid symbols represent calculated bulk compositions connected by solid tie lines. Open symbols are compositions of exsolved pyroxenes and host connected to bulk compositions by dashed tie lines. Heavy dashed curve on Fe-rich side of quadrilateral is polythermal boundary of "forbidden zone" at 5 kbar after Lindsley (1983).

Table 3. Temperatures of magmatic crystallization and cessation of major exsolution for pyroxenes from the Puttuaaluk Lake area

Sample	Exsolution type	Temperature of pyroxene crystallization		Temperature of cessation of exsolution based on	
		Ca-poor**	Ca-rich**	lamellae**	host**
PL-11*	1	686 [0.59]	765 [0.45]		
PL-150	1	821 [0.34]	710 [0.23]		
IR-31	2	1007 [0.52]		760 [0.37]	692 [0.53]
PL-117	2	1011 [0.49]	906 [0.39]	704 [0.35]	773 [0.50]
PL-211	2	997 [0.55]		734 [0.43]	723 [0.57]
PL-153	2	1117 [0.44]		649 [0.32]	711 [0.45]
PL-210	3	1009 [0.61]		557 [0.50]	866 [0.63]
PL-187*	3	956 [0.77]	950 [0.72]	688 [0.69]	710 [0.78]
PL-191	3	976 [0.76]	1021 [0.73]	658 [0.69]	817 [0.77]

Note: Temperatures in degrees celsius at 3-kbar pressure.
* Samples saturated with augite.
** [ ] = Fe/(Fe + Mg) for bulk composition, lamellae, or host as indicated.

erogeneous nucleation is favored at high temperatures and slow cooling, whereas homogeneous nucleation is favored by lower temperatures and intermediate cooling rates of a fairly narrow temperature range. All of the samples containing type 3 pyroxenes (PL-187, PL-191, PL-210) were collected near the margin of the anorthositic massif (Fig. 1) and are fine to medium grained, suggesting a moderate cooling rate. By comparison, samples with type 2 pyroxenes (IR-31, PL-117, PL-153, PL-211) come from the interior of the massif and are coarse to medium grained, indicating slower cooling. Results of pyroxene thermometry presented in the following section suggest that the type 3 pyroxenes crystallized at somewhat lower temperatures than the type 2 pyroxenes. These observations support the suggestion that the type 2 pyroxenes are products of heterogeneous nucleation and the type 3 of homogeneous nucleation, and that the observed differences in exsolution can be explained in this manner. Furthermore, regular pigeonite lamellae exsolved from irregular augite in type 2 pyroxenes were initiated at a lower temperature and probably under conditions of more rapidly falling temperature than that experienced by the host originally. Hence, the pigeonite lamellae underwent homogeneous nucleation, in contrast to the host augite formed through heterogeneous nucleation.

Pyroxene thermometry and exsolution chronology

Temperatures of magmatic crystallization and temperatures marking the cessation of coarse exsolution have been estimated using the pyroxene thermometer of Lindsley and Andersen (1983). Using this thermometer an understanding can be gained of the cooling history of these pyroxenes and the rocks that include them. The nine samples investigated are plotted in Figure 7, which shows the pyroxene quadrilateral and isotherms of Lindsley and Andersen (1983). Reconstructed bulk compositions, compositions of coarse "001" and "100" augite lamellae, and host compositions are plotted in Figure 7. Estimates of temperatures of crystallization and of cessation of exsolution are given in Table 3. Only two of the nine samples contain primary augite, so all but two of the *crystallization* temperatures recorded in Table 3 are minimum temperatures of crystallization. Temperature estimates for cessation of exsolution of coarse "001" and "100" augite given in Table 3 are based on both lamellar and associated host compositions. Close agreement between host and lamellar temperatures suggests that the estimates are reliable. Disagreement, as in the case of PL-191 and especially PL-210, is probably the result of finely exsolved augite in the host which is not resolvable with the electron-microprobe beam. These fine lamellae raise the Wo content and hence the temperature estimate for these host regions. Discounting the temperatures associated with host regions of PL-191 and PL-210, cessation of augite exsolution took place in the temperature range from 773 to 557°C for type 2 and type 3 pyroxenes. Fine pigeonite exsolution found within "001" augite and usually not resolvable with the electron beam, probably took place down to lower temperatures.

Temperature of crystallization plotted versus 100Fe/(Fe + Mg), for Ca-poor pyroxenes in Figure 8, shows a sharp distinction between inverted pigeonites and primary orthopyroxenes. Inverted pigeonites form a high-temperature-of-crystallization trend with temperature falling as Fe/(Fe + Mg) increases, whereas primary orthopyroxenes plot at lower temperature. The surprisingly low temperatures of crystallization for PL-150 and especially PL-11 may reflect granule exsolution of augite from orthopyroxene that was not accounted for, even though these orthopyroxenes appeared to be primary and contain only (100) augite exsolution. Alternatively, postcrystallization reequilibration at submagmatic temperatures may have occurred in the form of (Mg,Fe) ⇌ Ca exchange. The experiments of Lindsley and Andersen (1983) suggest such an explanation for submagmatic temperatures for some Skaergaard augites. Sample IR-31, which has exsolved

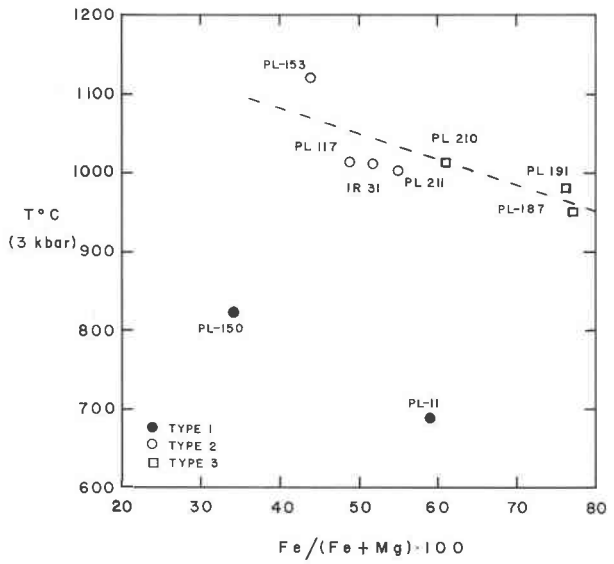

Fig. 8. Temperature of crystallization at 3-kbar pressure plotted against 100Fe/(Fe + Mg) for Puttuaaluk Lake pyroxenes. Pyroxene bulk compositions were reconstructed from host and lamellar compositions as described in the text, with the exception of PL-11 and PL-150, which contain only fine (100) augite exsolution. Temperatures are minimum temperatures except for PL-11 and PL-187, which are saturated with augite. High-temperature crystallization trend is that of Type 2 and Type 3 pyroxenes. Dashed line is visually fit to the data. Pyroxenes from PL-11 and PL-150 plotting at low temperature are Type 1 pyroxenes. See text for discussion.

pyroxene characteristic of both type 1 and type 2 pyroxenes, may possibly have crystallized both primary orthopyroxene and primary pigeonite since the inferred temperature is very close to the minimum temperature for pigeonite of this Fe/(Fe + Mg) ratio (Lindsley, pers. comm., 1985).

Jaffe (pers. comm., 1984) has suggested that by using the relationships obtained for Bushveld specimens as illustrated in Figure 9 and Figure 10 of Robinson et al. (1977) and the angular relationships for host and lamellae reported in Appendix 1, it can be shown that coarse exsolution began at a temperature above the $C2/c \rightleftharpoons P2_1/c$ inversion point. According to the data of Robinson et al. and assuming a reasonable β angle for the pigeonite host of from 109 to 110°, Aug I $\wedge$ $\mathbf{c}_{Pig} = 108°$ and Aug "100" $\wedge$ $\mathbf{c}_{Pig} = -6°$ indicate $a_{Pig} > a_{Aug}$ and $c_{pig} > c_{Aug}$, which is possible only above a temperature of 800°C, the approximate $C2/c \rightleftharpoons P2_1/c$ inversion temperature (see Figs. 9 and 10, Robinson et al., 1977).

The experiments of Lindsley and Andersen (1983) may also be used as an independent check on the pressures of crystallization for Nain anorthositic rocks. The two most Fe-rich inverted pigeonites, having the lowest temperatures of crystallization, are PL-191 and PL-187. PL-191 contains the assemblage inverted pigeonite + fayalite + minor augite and PL-187 contains the same assemblage with the addition of quartz (see App. 1). It is apparent from these assemblages that Fe-rich orthopyroxene (inverted pigeonite) is reaching its limit of stability and is giving way to augite + olivine + quartz. These pyroxenes plot just to the left of Lindsley's polythermal boundary for the "forbidden zone" at 5 kbar (Fig. 7) and hence indicate maximum pressures of 3 to 4 kbar. Hence, these pressures based on pyroxene composition confirm the pressure estimates of Berg (1977 and pers. comm., 1983) based on metamorphic mineral assemblages in the contact aureole of the anorthositic Nain complex.

In summary, most Ca-poor pyroxenes crystallized as pigeonite at temperatures around 1100 to 1000°C (minimum temperatures for most samples) at 3–4-kbar pressure and underwent exsolution of augite by a mechanism of nucleation and growth. Coarse exsolution began above about 800°C, the approximate $C2/c \rightleftharpoons P2_1/c$ inversion temperature, and continued down to temperatures perhaps below 600°C. The formation of stacking faults, which initiated the transformation from pigeonite to orthopyroxene, occurred as the temperature fell and the resultant strain on the pigeonite-augite phase boundary increased. The pigeonite to orthopyroxene transition was not always complete as witnessed by small, metastable patches of pigeonite sandwiched between augite lamellae in type 3 pyroxenes. Pigeonite probably began exsolving from "001" augite lamellae before inversion and continued to form as fine metastable exsolution even after the host became orthopyroxene. The lower temperature limit of pigeonite exsolution is not known.

Acknowledgments

The author wishes to thank S. A. Morse for providing both the opportunity and financial support for field work in Labrador. H. W. Jaffe and P. W. Ollila reviewed an early version of the manuscript and contributed to its improvement. J. S. Huebner and D. H. Lindsley also provided perceptive reviews. M. D. Leonard assisted with the electron-microprobe facility at the University of Massachusetts. To each of these persons the author gratefully extends his thanks. Support was provided by the Geological Society of America grant-in-aid 2245-77 to W. A. Ranson and by Earth Science Division, National Science Foundation Grants EAR 73-00667 and EAR 74-22509, both to S. A. Morse.

References

Albee, A.L., and Ray, Lily. (1970) Correction factors for electron probe microanalysis of silicates, oxides, carbonates, phosphates, and sulfates. Analytical Chemistry, 42, 1408–1414.

Bence, A.E., and Albee, A.L. (1968) Empirical correction factors for the electron microprobe analysis of silicates and oxides. Journal of Geology, 76, 382–403.

Berg, J.H. (1977) Regional geobarometry in the contact aureoles of the anorthositic Nain complex, Labrador. Journal of Petrology, 18, 399–430.

Bollman, W, and Nissen, H.-U. (1968) A study of optimal phase boundaries: The case of exsolved alkali feldspar. Acta Crystallographica, A24, 546–557.

Brown, G.M. (1968) Experimental studies of inversion relations in natural pigeonitic pyroxenes. Carnegie Institution of Washington Year Book 66, 347–353.

Buseck, P.R., Nord, G.L., Jr., and Veblen, D.R. (1980) Subsolidus phenomena in pyroxenes. Mineralogical Society of America Reviews in Mineralogy, 7, 117–211.

Champness, P.E., and Copley, P.A. (1976) The transformation of pigeonite to orthopyroxene. In H.-R. Wenk, Ed. Electron

Microscopy in Mineralogy, 228–233. Springer-Verlag, New York.
Champness, P.E., and Lorimer, G.W. (1976) Exsolution in silicates. In H.-R. Wenk, Ed. Electron microscopy in mineralogy, 174–204. Springer-Verlag, New York.
Coe, R.S., and Kirby, S.H. (1975) The orthoenstatite to clinoenstatite transformation by shearing and reversion by annealing: Mechanism and potential applications. Contributions to Mineralogy and Petrology, 52, 29–55.
Hess, H.H. (1941) Pyroxenes of common mafic magmas. American Mineralogist, 26, 515–535, 573–594.
Hess, H.H., and Phillips, A.H. (1940) Optical properties and chemical composition of magnesian orthopyroxenes. American Mineralogist, 25, 271–285.
Huebner, J.S., and Turnock, A.C. (1980) The melting relations at 1 bar of pyroxenes composed largely of Ca-, Mg-, and Fe-bearing components. American Mineralogist, 65, 225–271.
Huntington, H.D. (1980) Anorthositic and related rocks from Nukasorsuktokh Island, Labrador. Ph.D. thesis, University of Masachusetts, Amherst.
Jaffe, H.W., and Jaffe, E.B. (1973) Bedrock geology of the Monroe quadrangle, New York. New York State Museum and Science Service, Map and Chart Series No. 20, Albany, New York.
Jaffe, H.W., Robinson, Peter, Tracy, R.J., and Ross, Malcolm. (1975) Orientation of pigeonite lamellae in metamorphic augite: Correlation with composition and calculated optimal phase boundaries. American Mineralogist, 60, 9–28.
Lindsley, D.H. (1983) Pyroxene thermometry. American Mineralogist, 68, 477–493.
Lindsley, D.H., and Andersen, D.J. (1983) A two-pyroxene thermometer. Proceedings of the Thirteenth Lunar and Planetary Science Conference, Part 2. Journal of Geophysical Research, 88, Supplement, A887–A906.
Lindsley, D.H., Mac Gregor, I.D., and Davis, B.T.C. (1964) Synthesis and stability of ferrosilite. Carnegie Institution of Washington Year Book 63, 174–176.
Morimoto, N., and Koto, K. (1969) The crystal structure of orthoenstatite. Zeitschrift für Kristallographie, 129, 65–83.
Poldervaart, Arie, and Hess, H.H. (1951) Pyroxene in the crystallization of basaltic magma. Journal of Geology, 59, 472–489.
Ranson, W.A. (1978) Exsolution in Ca-poor pyroxenes from anorthositic rocks of the Nain complex, Labrador. Geological Society of America Abstracts with Programs, 10, 476.
——— (1979) Anorthosites of diverse magma type in the Puttuaaluk Lake area, Nain complex, Labrador. Ph.D. thesis, University of Massachusetts, Amherst.
——— (1981) Anorthosites of diverse magma types in the Puttuaaluk Lake area, Nain complex, Labrador. Canadian Journal of Earth Sciences, 18, 26–41.
Rietmeijer, F.J.M. (1979) Pyroxenes from iron-rich igneous rocks in Rogaland, S.W. Norway. Ph.D. thesis, University of Utrecht, Netherlands.
Robinson, Peter. (1980) The composition space of terrestrial pyroxenes—Internal and external limits. Mineralogical Society of America Reviews in Mineralogy, 7, 419–494.
Robinson, Peter, Jaffe, H.W., Ross, Malcolm, and Klein, Cornelis, Jr. (1971) Orientation of exsolution lamellae in clinopyroxenes and clinoamphiboles: Consideration of optimal phase boundaries. American Mineralogist, 56, 909–939.
Robinson, Peter, Ross, Malcolm, Nord, G.L., Jr., Smyth, J.R., and Jaffe, H.W. (1977) Exsolution lamellae in augite and pigeonite: Fossil indicators of lattice parameters at high temperature and pressure. American Mineralogist, 62, 857–873.
Ross, Malcolm, and Huebner, J.S. (1979) Temperature-composition relationships between naturally occurring augite, pigeonite, and orthopyroxene at one bar pressure. American Mineralogist, 64, 1133–1155.
Smith, Douglas. (1974) Pyroxene-olivine-quartz assemblages in rocks associated with the Nain anorthosite massif, Labrador. Journal of Petrology, 15, 58–78.
Stephenson, D.A., Sclar, C.B., and Smith, J.V. (1966) Unit cell volumes of synthetic orthoenstatite and low clinoenstatite. Mineralogical Magazine, 35, 838–846.
Wager, L.R., and Brown, G.M. (1967) Layered igneous rocks. Freeman, San Francisco.
Yund, R.A., and McCallister, R.H. (1970) Kinetics and mechanics of exsolution. Chemical Geology, 6, 5–30.

Manuscript received September 11, 1985
Manuscript accepted July 8, 1986

Appendix 1. Sample description

PL-11

A medium- to fine-grained gabbroic anorthosite with 60% andesine (An_{44}), 26% augite, 10% type 1 orthopyroxene, 2% Fe-Ti oxides, 2% hornblende and trace biotite. The two pyroxenes are very closely associated and are commonly intergrown. Orthopyroxene [0.59][1] forms fine-grained crystals interstitial to coarser plagioclase. Exsolved pyroxene consists of fine (<0.1 μm thick) (100) augite lamellae characteristic of type 1 orthopyroxene. Augite [0.46] also forms fine-grained crystals interstitial to coarser plagioclase and contains exsolved orthopyroxene and pigeonite. Exsolved pigeonite has orientation "001" with respect to the host augite and consists of 1–2-μm-thick lamellae generally continuous across host crystals but tapered at the ends ("001" $\wedge$ **c** = 113°). Orthopyroxene lamellae are about 0.2 μm in width, have a (100) orientation, and are discontinuous across the host augite crystals.

PL-150

Coarse- to medium-grained leuconorite with 60% labradorite (An_{53}) (including antiperthite), 38% type 1 orthopyroxene, 1% augite, 1% Fe-Ti oxides. Coarse-grained, subhedral orthopyroxenes in this rock contain fine (<1 μm) augite lamellae oriented parallel to (100) of the host. Fine oxide exsolution lamellae are also present with an orientation of (100). Fine-grained, anhedral augite crystals occur at the margins of large orthopyroxenes or more rarely are included by orthopyroxene, suggesting an origin for the augite by granule exsolution. Augite contains fine (<1 μm) (100) lamellae of orthopyroxene.

IR-31

Medium-grained leuconorite with 85% andesine (An_{39}), 10% orthopyroxene, 4% augite, 1% magnetite. The orthopyroxenes bear similarity to both type 1 and type 2 proxenes. Many appear to be primary and contain only fine (100) augite lamellae. Other examples have augite granules within and adjacent to the orthopyroxene crystals, making accurate determination of composition and classification difficult. Augite also occurs as an interstitial phase apart from orthopyroxene and has two sets of pigeonite lamellae with orientations of "001" and "100" ("001" $\wedge$ "100" = 119°). Lamellae oriented at "001" are 2 to 3 μm thick and have an indistict, granular appearance. "100" lamellae are fine (1 μm) and discontinuous along the length of the host.

PL-117

Medium- to coarse-grained, oxide-rich leuconorite with 77% labradorite (An_{56}), 10% type 2 inverted pigeonite, 5% augite, 5% ilmenite, 3% quartz-plagioclase intergrowths, 1% biotite. Inverted pigeonite [0.50] forms coarse-grained (5–7 mm) and fine-grained (1–3 mm) crystals containing coarse (up to 0.1 mm in width) irregular lamellae and blebs of augite of nonuniform orientation.

[1] Values in brackets are the atomic ratio $(Fe_t + Mn)/(Mg + Fe_t + Mn)$.

Some inverted pigeonites also contain fine (100) augite lamellae more characteristic of type 1 low-Ca pyroxenes. Augite crystals [0.38] form at the margins of, or within, large inverted pigeonite crystals and are anhedral. Three sets of "001" pigeonite lamellae were observed in host augite: a coarse set (10 μm thick) continuous across the grains ("001" $\wedge$ **c** = 102°), a fine set (0.05 to 1 μm thick; "001" $\wedge$ **c** = 108°), and a very fine set (0.01 μm thick). In addition, fine (1–2 μm) discontinuous (100) lamellae of orthopyroxene are present. Yet another set of exsolution lamellae with a "100" orientation is barely resolvable with the microscope and probably constitutes a fourth set of pigeonite lamellae.

PL-211

Coarse-grained leuconorite with 80% andesine (An_{46}), 14% type 2 inverted pigeonite, 3% Fe-Ti oxides, 3% K-feldspar. Inverted pigeonite [0.57] forms coarse (5–8 mm), anhedral crystals containing abundant exsolved augite in the form of irregular lamellae, blebs, and granules adjoining the host margins. In thin section, irregular lamellae have a variable orientation with respect to the **c** axis depending on the orientation of the host crystal in relation to the plane of the thin section. However, in immersion mounts, cleavage plates have augite lamellae perpendicular to the **c** axis. Broad (40–50 μm) augite lamellae with irregular boundaries contain fine (1–3 μm) pigeonite lamellae with "001" orientations and equally fine (100) orthopyroxene lamellae. Granules of augite exhibit the same patterns of pigeonite exsolution.

PL-153

Medium-grained, oxide-rich anorthosite with 85% labradorite (An_{53}), 8% type 2 inverted pigeonite, 6% ilmenite, 1% augite. Inverted pigeonite forms crystals between 0.5 and 1.0 mm in length and contains irregular lamellae and blebs of exsolved augite at nonuniform orientations typical of type 2 low-Ca pyroxenes. Exsolved augite blebs and lamellae range in width from 40 to 60 μm. Equant augite crystals averaging about 0.1 mm across occur at the margins of large inverted pigeonites and may represent the result of granule exsolution. Augite contains both "100" and "001" pigeonite lamellae. "001" lamellae are continuous and 1–2 μm in width, whereas "100" lamellae are discontinuous and <1 μm in width.

PL-210

Medium- to fine-grained leuconorite with 64% labradorite (An_{51}), 30% type 3 inverted pigeonite, 2% augite, 4% Fe-Ti oxides, trace apatite. Inverted pigeonite forms crystals up to 2 mm in length containing broad (30 μm) "001" augite lamellae (Aug I $\wedge$ $\mathbf{c}_{Pig}$ = 107°). Augite lamellae contain fine pigeonite lamellae parallel to "001" and "100" of the augite, although the "100" set is rare. Stacking faults or unresolvable lamellae of uncertain composition cut the host inverted pigeonite but do not penetrate the augite lamellae. Rectangular patches of uninverted pigeonite are constrained between adjacent broad augite lamellae and are a common characteristic of these pyroxenes.

PL-187

Medium-grained monzodiorite with 50% andesine (An_{37}) (including antiperthite), 25% perthite, 7% hornblende, 4% augite, 3% type 3 inverted pigeonite, 5% fayalite ($Fo_{8.2}Fa_{90.2}Te_{1.6}$), 5% quartz, 1% apatite. Inverted pigeonite crystals (0.5–1.0 mm in length) have exsolved "001" augite lamellae (Aug I) 30 to 40 μm in thickness (Aug I $\wedge$ $\mathbf{c}_{Pig}$ = 108°). Most augite lamellae are continuous and have sharp straight boundaries, although irregular lamellae and blebs of augite do occur in some inverted pigeonite. Vertical patches of augite connect adjacent "001" augite lamellae in some inverted pigeonite crystals. Discrete augite crystals, which are closely associated with inverted pigeonite, have two sets of "001" pigeonite lamellae, a set of coarser ($\sim$0.8 μm), continuous lamellae ("001" $\wedge$ **c** = 108°) and a set of fine (<0.1 μm) discontinuous lamellae across the host crystal ("001" $\wedge$ **c** = 112°). A third set consists of pigeonite lamellae that have a "100" orientation and are thin (<1 μm) and less common than the "001" lamellae. Composite grains of augite and inverted pigeonite occur, usually consisting of large patches of inverted pigeonite contained in augite.

PL-191

Fine-grained ferrodiorite with 52% andesine (An_{33}) (including minor antiperthite), 39% type 3 inverted pigeonite, 6% Fe-rich olivine, 4% Fe-Ti oxides; traces of clinopyroxene, hornblende, K-feldspar. Inverted pigeonite crystals are irregularly shaped, average about 1 mm in length, and contain broad (40–50 μm), evenly spaced and sharply bounded "001" augite lamellae (Aug I). These lamellae are usually continuous across the host and are tapered (Aug I $\wedge$ $\mathbf{c}_{Pig}$ = 108°). Exsolving from broad "001" augite lamellae are two sets of fine (<1 μm) pigeonite lamellae with slightly different "001" orientations. A second 6–10-μm set of augite lamellae (Aug "100") have a "100" orientation and are restricted to portions of crystals where there are no Aug I lamellae (Aug "100" $\wedge$ $\mathbf{c}_{Pig}$ = -6°). Aug "100" lamellae stop abruptly at the phase boundaries of Aug I lamellae. Finally, a third, narrower (3–5 μm) set of augite lamellae (Aug II) has orientation of "001" but occurs at a slightly steeper angle than Aug I lamellae (Aug II $\wedge$ $\mathbf{c}_{Pig}$ = 109°). Fine stacking faults and accompanying fine lamellae of augite (?) oriented parallel to (100) of the host are bent as they pass from host into broad augite lamellae.

Minor interstitial clinopyroxene has two sets of exsolved pigeonite lamellae with a "001" orientation: a coarser set with 2-μm-thick lamellae ("001" $\wedge$ **c** = 110°) and a finer set with 0.5-μm-thick lamellae ("001" $\wedge$ **c** = 114°). Orthopyroxene lamellae parallel to (100) are also present and are 1–2 μm in width.